IEEE Access
Multidisciplinary | Rapid Review | Open Access Journal

Received December 22, 2019, accepted January 4, 2020, date of publication January 13, 2020, date of current version January 28, 2020.

Digital Object Identifier 10.1109/ACCESS.2020.2966272

Internet of Medical Things (IoMT) Assisted Vertebral Tumor Prediction Using Heuristic Hock Transformation Based Gautschi Model–A Numerical Approach

HASSAN FOUAD[1,2], AZZA S. HASSANEIN[2], AHMED M. SOLIMAN[2], AND HAYTHAM AL-FEEL[3]

[1]College of Applied Medical Science, King Saud University, Riyadh 11433, Saudi Arabia
[2]Biomedical Engineering Department, Faculty of Engineering, Helwan University, Cairo 11795, Egypt
[3]Faculty of Computers & Information, Fayoum University, Fayoum 63514, Egypt

Corresponding author: Hassan Fouad (menhfef@ksu.edu.sa)

This work was funded by Researchers Supporting Project number (RSP-2019/117), King Saud University, Riyadh, Saudi Arabia.

ABSTRACT A vertebral tumor is a category of spinal tumor which influence the bones or vertebrae of the spine in the human body system. The Spinal tumors that start inside the spinal string or the covering of the spinal line (dura) are called spinal rope tumors. Furthermore, the tumors that influence the vertebrae have frequently spread (metastasized) from the malignant growths in different parts of the body which is erratic with increasing the precision outcomes with the presence of medical instruments. Moreover, there are a few types of tumors that start inside the bones of the spine, for instance, such as chordoma, chondrosarcoma, osteosarcoma, plasmacytoma and Ewing's sarcoma. A vertebral tumor can influence the neurological capacity by pressing on the spinal string or nerve roots closer. In this paper, the vertebral tumor is analysed using Heuristic Hock Transformation Based Gautschi's-Blur Model (HHTGM) as a numerical approach. As these tumors developed inside the bone, they may likewise lead to torment, vertebral breaks or spinal precariousness which has been further examined in this research using Internet of Medical things (IoMT) Platform. Whether harmful or not, a vertebral tumor can be hazardous and cause perpetual incapacity has been tentative and experimentally analysed in accordance with HLC, CTM, LM, and CFRM methods, moreover HHTGM in this research explored the best results with 95.8% efficiency and 98.66 % of precision when compared with these methods.

INDEX TERMS Gautschi's-Blur model, IoMT, cervical spine lumbar vertebral, malignant growth.

I. INTRODUCTION

The majority of the vertebras in the human spinal column (other than C1, C2 and sacrum) are very similar, especially when compared among the vertebras in each spinal segment (cervical, thoracic and lumbar) [1]. In addition, as various image surveys on the back usually consist of several image sets, where radiologists will manually annotate the vertebra with a mark in a sagittal image to help navigate, as radiologist's shift attention across the different image series. This helps the radiologist not to have re-identified all vertebrates whenever another series of photographs are shown [2].

The associate editor coordinating the review of this manuscript and approving it for publication was Wei Wei.

Many research groups for both computer tomography (CT) and magnetic resonance (MR) have already proposed for the identification and marking of image data showing the backbone [3]. Further, several images required training data in the form of completely segmented vertebras, whereas others with bounding boxes and only a few that involve each vertebras location.

However, only some of the latest work has been called deep learning concepts where annotations as training information were used for this reason [4]. Several researches show that the clinicians could train deeper pipelines for identification of vertebras in the sagittal MR images by means of annotations of spine labels in a single format database which is accessible for detection and labeling.

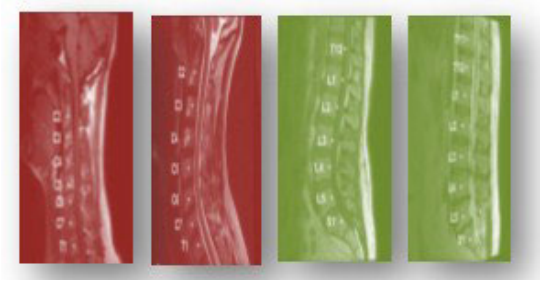

(a) Inaccurate Cervical. (b) Accurate Cervical. (c) Inaccurate Lumbar. (d) Accurate Lumbar.

FIGURE 1. An example of lumbar and cervical case with the label spine data's placed in an inaccurate way (a) and (c) have not been placed in the centered position (b) and (d) are placed accurately.

Regarding recent MR cases of spine labels which indicate the lumbar and cervical spine, the regional image photo was examined [5]. Once the relevant image information and the tags were established, subsequent de-identification compliant was exported. Their position was not always accurate as shown in the Figure 1 (a) and (b) or consistent because the annotated spine tag was initially given to aid navigation [6]. A manual quality assurance process was therefore necessary to ensure all retained cases could correctly locate as shown in the Figure 1 (c) and (d) and place all spine labels on their respective backbones [7].

It is worth noting that not all cases have photographs of T1 and T2 as well as the number of vertebrae marked may vary [8]. The normal user scenario of the column labeling required the placing of backbone labels in an image, normally the mid-slice in a sagittal image set. This choice of format, for instance for scoliosis, decreases the utility of proposed pipelines marginally [9]. Nonetheless, this can easily be done in an actual implementation, to guarantee a consistent resolution of all images, the image data were resampled to $1/1$ mm^2. Finally, the data were allegedly broken down into three groups, including learning, verification and testing (60% 20% 20%).

This study was conducted in retrospect, using photo studies which are already carried out by several researchers in the field. Thus, the local institutional review committee ruled the study exempt and informed consent was rejected. Another important aspect of scoliosis assessment is often vertebral rotation. Several techniques for evaluating the radiographic spin [10] from the vertebral were developed by locating the sites of the posterior anterior radiograph [11]. In addition to the considerable accuracy of observers in these techniques, however, pedicle screws obscure those points of reference which are needed to measure rotation after surgery. The evaluation is calculated directly from biplane radiographs where the 3D vertebral orientations are located [12].

Presently, the significant growth of the vertebral Internet of medical things (IoMT) technology provides access to medical information opportunities and challenges. Because the information used is massive, which is big data, computing resources must be distributed. The data used are essential and heterogeneous in nature since the information is distributed via a cloud computing platform which is the software approach to dealing with this data using IoT platform with Spinal cord (SC) PhotoPlethysmoGram (PPG) [13]. These are developed with the hybrid data in mind and the heterogeneous data is being processed via a cloud platform for the feasibility study. In medical applications, IoMT data in healthcare are used and health monitoring Sensors are used to collect data from the patients. To evaluate operating performance, the data collection is done using a hardwired approach using high precision sensors with high compression sensing for image acquisition analysis [14].

IoMT trust is often limited by the supply of energy. Thus, the machines are mounted where power is terrifying and there is no possible human interference. The energy collection is thus required to regenerate. Based on the problem discussion and survey prominent, objectives have been taken in this research as given below:

- A new method for the identification of multiple bone lesions in an accurate and effective manner.
- The auto crop is then added to the spine section using vertical screening and normal disposal with high precision.
- The border segmentation analysis for Gautschi's-Blur corrections and Heuristic Hock Transformations (HHTGM) is defined by the limits between the foreground and background to analyse vertebral pose.
- Further the vertebral breaks or spinal precariousness which has been further examined in this research using Internet of Medical things (IoMT) Platform with experimental results.

II. BACKGROUND SURVEY

The neck (cervical spinal cord) is a moving part of the body and is vulnerable to damage. Incorrect diagnoses of this image can lead to long-term serious consequences in patients suspected of cervical spine damage. The overall objective mentioned in this design is the usage of computer-based detection system that helps a doctor to diagnose a patient's injury properly. Here the authors present a procedure within 90 lateral cervical X-rays in which the corners of the cervical vertebras may be located and [15] Haar-Like Characteristics (HLC) were calculated by means of image patches using fluoroscopic analysis [16], where each of which votes in a favor of a possible vertebral corner position. Two-dimensional kernel density estimation is used to aggregate the location of the corner. This approach shows promising results in the detection of corners with an average error of 6.15 pixels.

In cases of severe osteoporosis, thoracolumbar spine vertebral body fractures can occur without trauma. Initially, acute spinal fractures can be diagnosed, and the stability of the individual fractures is advised with a standardized diagnostic algorithm. The aim of the treatment is to ensure relatively painless movement while preserving vertebral alignment. For patients with stable fractures a Conservative Therapy

Method (CTM) [17] was introduced. The treatment technique is to reduce the invasive cement enhancement for persistent pain, reduced mobility, or improves kyphotic misalignment. A more complex therapy concept such as hybrid stabilization must be selected in cases of unstable fracture morphology. A lot of experience for revision operation is required and, in such cases, it could be necessary to reconstruct several segments, and the Platform should exceed the apex of kyphotic.

Twelve studies were conducted after an endemic investigation into the link between increasing density of spine-bone minerals and reducing the risk of vertebral fractures in postmenopausal women. They used logistic models (LM) in the fracture intervention study [18] to quantify the percentage of risk of alendronate vertebral fractures observed by increasing mineral density in the bone. For instance, the model estimated that therapies would decrease the risk of fractures by 20% because of the improvement of bone mineral density by 45%. In the fracture intervention study, increased concentration of minerals of spine bones was 16% less chance of alendronate spinal fractures [18].

This invention includes a vertebral implant to restore and/or keep the required disk space height and spinal orientation to an effect in a disk space. The implants have an extended base body which is generally fitted with lenses from upper and lower convex surfaces. On cross-sectional surfaces of the end walls, bears are given. Grooves between the bearing surfaces are provided on the upper and the lower surfaces. The implant can be prepared with a range of materials including metallic materials, synthetic materials, and polymeric materials, ceramic and Carbon Fibre Including Reinforced Materials (CFRM) [19]. These preferred materials used to produce implants which could reduce costs, increased service life and offered excellent physiological compatibility in the present invention. It is possible to select the non-metallic material as either significantly permanent, biodegradable or bio-erodible material.

The previous cervical spinal operations were all identified for the incidences for hernia and degenerative disc or cervical spondylosis. Anterior cervical procedures have been removed from this review for trauma, neoplasia or disease. Records have been obtained via the institution-wide electronic record search of 10 spine surgeons via surgical papers. The reports were subsequently reviewed in hospitals and medical maps. Intraoperative And Demographic Data (IADD) [20] is registered for repair. The control of arterial bleeding is initially controlled by homeostasis; however, the repair or ligation must also be considered. The other three patients were primarily repaired or tied up, and no complications were observed. Based on the various surveys, this research focuses on the vertebral tumor which can influence the neurological capacity by pushing on the spinal string or nerve roots close is eccentric using Heuristic Hock Transformation Based Gautschi's-Blur Model (HHTGM) a numerical approach. Further vertebral breaks or spinal precariousness has been analysed using Internet of Medical things (IoMT) Platform for experimental analysis.

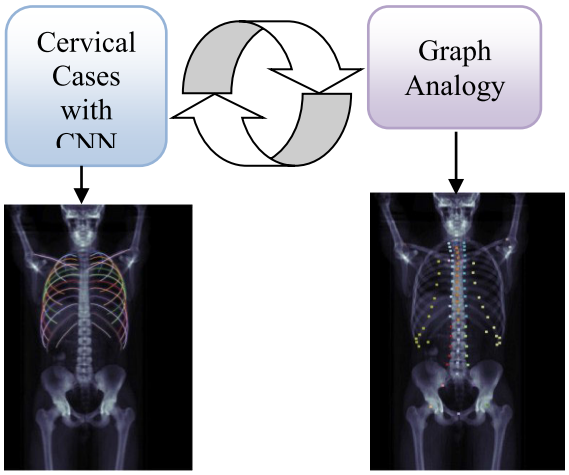

FIGURE 2. Labeling pipeline and detection setup for cervical vertebra.

III. HEURISTIC HOCK TRANSFORMATION BASED GAUTSCHI'S-BLUR MODEL (HHTGM): A NUMERICAL APPROACH.

In this method, there were two separate pipelines for identification and marking, one for the lumbar and the other for the cervical case. Nevertheless, two neural tube convolution neural networks (CNNs) have been designed to detect possible vertebras in the same way, respectively; one general cervical/lumbar vertebra detectors and the other one unique S1/C2 vertebral detector, accompanied by a partial graphic. Any thoracic vertebrae shown in the images would also be detected by the general vertebral detectors as taken from the data sets [21] with dataset numbers of 2, 3, 5, 7, 9, 12, 13, and 15.

All CNNs are similarly connected to two convolutions (C) layers followed by a multi perceptron (MP) layer with 2 additional C layers and a MP layer with 2 fully integrated convolution layers (FC) in front of the following output layers. Image patches are removed from the image as shown in the Figure 2 and fade into both the cervix as well as C2 CNNs, the only patches of the vertebrae that provide precise pixel detections.The centroids of the detections have been maintained and supplied with a partially derived graphic template that follows the connecting components analysis of the detection charts, which rejects false positive detection and marks remaining detection. The final output of the annotated column labeling is thus given.

The solution proposed has been based on the Generalized Hock Transformation Using Gautschi's-Blur Model (GHTGM) to obtain the edge images which are precondition for the HT. Furthermore, the Canny edge detector has been used. Internet of Medical Things (IoMT) Platform with transformation technology is planned to be used by the proposed Heuristic Hock Transformation Based Gautschi's-Blur Model for experimental analysis of various optimization parameters. The transformation platform is cloud-based server and the vertebral sensors are installed in

hospitals for analysing the patient's health data which are recorded by the sensors. The sensors monitor and transmit data on a regular basis, it can be tracked anywhere with the help of PC or even through the mobile phone as analysed in the experimental cases in this paper.

A. MATHEMATICAL ANALYSIS-1: HOCK TRANSFORM WITH FOURIER SERIES

The mathematically formulated vector function that defines the points along with the curve in two orthonormal axes by means of components and it is expressed mathematically in the following Equation (1) as follows:

$$\bar{B}(s) = b_Y(s)v_Y + b_X(s)v_X \tag{1}$$

As inferred from the Equation (1), where the two orthonormal vectors are $v_Y = [1, 0]$ and $v_X = [0, 1]$, where S∋ $(0,2\alpha)$ varies the curve from the a range of points. The b_Y(s) and b_X(s) components can be represented through the Fourier expansion with constant fator α, according to Fourier theory following expansion, which is represented in the Equation (2) as follows:

$$\begin{bmatrix} b_y(s) \\ b_x(s) \end{bmatrix} = \sum_{j=1}^{j=m} \begin{bmatrix} c_{yl} & d_{yl} \\ c_{xl} & d_{xl} \end{bmatrix} \begin{bmatrix} \sin(ls) \\ \cos(ls) \end{bmatrix} \tag{2}$$

From the computation in the Equation (2) Where m is the peak c(s) frequency, the harmonic number is l. Fourier descriptors (FDs) that may be calculated from the $c_{yl}, d_{yl}, c_{xl}, d_{xl}$ Coefficients which are mathematically computed using a discrete approximation as represented as in the trignomentric form as follows:

$$c_{yl} = \frac{2}{n}\sum_{j=1}^{n} y_j \sin(j\frac{2\alpha}{n}l) \tag{3}$$

$$d_{yl} = \frac{2}{n}\sum_{j=1}^{n} y_j \cos(j\frac{2\alpha}{n}l) \tag{4}$$

$$c_{xl} = \frac{2}{n}\sum_{j=1}^{n} x_j \sin(j\frac{2\alpha}{n}l) \tag{5}$$

$$d_{xl} = \frac{2}{n}\sum_{j=1}^{n} x_j \cos(j\frac{2\alpha}{n}l) \tag{6}$$

As denoted in the Equation 3, 4, 5, and 6, the following computation has been performed, where n is the sample point number, where y_j and x_j are the point $\frac{2\alpha}{n}$ Place in the curve. The curve obtained by translating, the scaling or turning similarities can be described in the y and x directions with its two components represented as follows:

$$\begin{bmatrix} b'_y(s) \\ b'_x(s) \end{bmatrix} = \begin{bmatrix} y_s \\ x_s \end{bmatrix} + w \begin{bmatrix} \sin\gamma & -cos\gamma \\ cos\gamma & sin\gamma \end{bmatrix} \begin{bmatrix} b_y(s) \\ b_x(s) \end{bmatrix} \tag{7}$$

where, w represents the scale factor, fix clockwise, and the translations described by y and x respectively which are represented by $b_y(s)$ and $b_x(s)$. The principle of the Heuristic Hock Transform (HHT) is used as a reference point in the HT space which is defined based on the position of the target contour. The HHT transformation, kernel has been defined as the HT derivative is shown as follows:

$$\mathrm{S(s,w,}\gamma) = w \begin{bmatrix} \sin\gamma & -cos\gamma \\ cos\gamma & sin\gamma \end{bmatrix} \begin{bmatrix} b_y(s) \\ b_x(s) \end{bmatrix} \tag{8}$$

Algorithm 1 Heuristic Hock Transform Using Fourier Series Method

1. ***Start Procedure: learning the features of Heuristic Hock Transform Using Fourier Series method of the algorithm.***
   Begin
2. ***Input:*** $b_Y(s)v_Y$ ***and*** $b_X(s)v_X$.
3. ***Output*** $\bar{B}(s)$
4. ***Ortho normal vectors are expanded using the Fourier series method.***
5. ***Calculate*** $\begin{bmatrix} b_y(s) \\ b_x(s) \end{bmatrix} \sum_{j=1}^{j=m} \begin{bmatrix} c_{yl} & d_{yl} \\ c_{xl} & d_{xl} \end{bmatrix} \begin{bmatrix} sin(ls) \\ cos(ls) \end{bmatrix}$
6. ***Calculate the coefficients of the equation*** c_{yl}, d_{yl}, c_{xl} ***and*** d_{xl}.
7. ***Calculate*** $\begin{bmatrix} y_s \\ x_s \end{bmatrix} = \begin{bmatrix} f_{yj} \\ f_{xj} \end{bmatrix} - S(s,w,\gamma)$
8. ***Finally, determine*** $\bar{B}(s)$
9. ***End begin***
10. ***Until repeat for all coefficients of the equation are calculated to determine the Fourier series method.***
11. ***End procedure***

As shown, the translation vector is calculated for every edge (f_{yj}, f_{xj}) and it is determined as follows:

$$\begin{bmatrix} y_s \\ x_s \end{bmatrix} = \begin{bmatrix} f_{yj} \\ f_{xj} \end{bmatrix} - \mathrm{S(s,w,}\gamma) \tag{9}$$

The accumulator array of the four dimensional HHT is defined as follows:

$$\begin{bmatrix} y_s \\ x_s \end{bmatrix} = \sum_{j\ni w} \sum_{s\ni\gamma} \begin{bmatrix} f_{yj} \\ f_{xj} \end{bmatrix} - \mathrm{S(s,\ w,}\gamma) \tag{10}$$

From the mathematical computation two orthonormal axes by means of components and it is expressed mathematically in the Heuristic Hock Transform using Fourier series method as shown in the Algorithm.1.

Step 1: Initiate the learning the features of Heuristic Hock Transform using Fourier series method of the algorithm

Step 2: Determine and execute the parameters of the following equations b_Y(s)v_Y, b_X(s)v_X and $\bar{B}$(s).

Step 3: Ortho normal vectors are expanded using the Fourier series method.

Step 4: Calculate $\begin{bmatrix} b_y(s) \\ b_x(s) \end{bmatrix} = \sum_{j=1}^{j=m} \begin{bmatrix} c_{yl} & d_{yl} \\ c_{xl} & d_{xl} \end{bmatrix} \begin{bmatrix} \sin(ls) \\ \cos(ls) \end{bmatrix}$

Step 5: Determine the coefficients of the equations c_{yl}, d_{yl}, c_{xl} *and* d_{xl}.

Step 6: Calculate $\begin{bmatrix} y_s \\ x_s \end{bmatrix} = \begin{bmatrix} f_{yj} \\ f_{xj} \end{bmatrix} - \mathrm{S(s,\ w,}\ \gamma)$

Step 7: Determine $\bar{B}$(s) until repeat for all coefficients of the equation is calculated to determine the Fourier series method effectiveness.

In our research, a new method for the identification of multiple bone lesions has been developed which includes:

- The auto crop is then added to the spine section by using vertical screening and normal disposal.

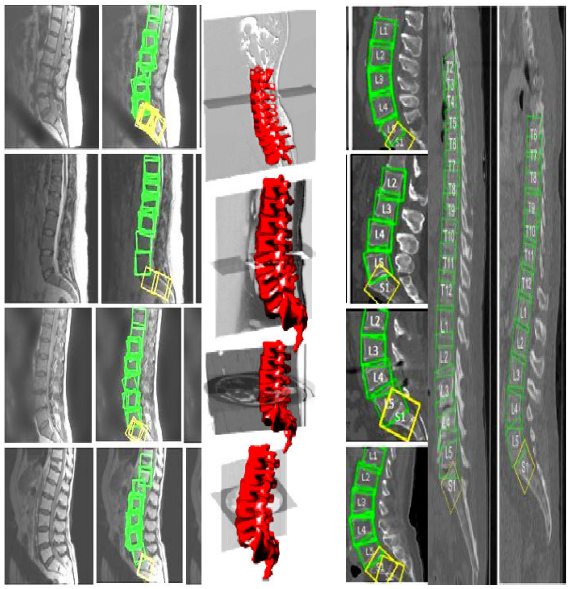

FIGURE 3. Detailed classification of (A) cervical and (B) lumbar cases of the vertebral spine.

- Secondly, we apply border segmentation consisting of Gautschi's-Blur corrections and heuristic hock transformations (HHTGM) to define the limits between the foreground and background. Thirdly, they are the vertebral poses.
- Then, with cervical bone 11 (T11) and lumbar bone 4 (L4) identification, we configure vertebral positions. To predict lesions, the identification of bone lesions have been experimentally analysed using Internet of Medical Things (IoMT). The algorithm of the IoMT takes data from the HHTGM.

The most important advantage of IoMT compatible vertebral spinal systems is providing information to people to gain a better view of their health outcomes. Vertebral spinal IoMT systems are in great demand as they offer greater exposure to individuals to make health decisions that are more educated. Because each vertebra is only a single point, the amount of image patches that could be used for learning has been increased, for both the sample pixels of each image has been split into four categories, based on the position of the spinal mark provided: vertebral center regions, inter vertebral disks, vertebral regions, and backbone regions as shown in the Figure 3. As shown in the Figure 3 (a) and (b), the pixels in the internal circular (yellow) regions are known as pixels centered in the vertebra, as pixels of intervertebral (green) pixels within the ellipsoidal (red) zone and as pixels of the background pixels within the outer circle (red) region. The regions of the center of the vertebral cell have been measured by the circulation size of smaller areas around each spine marking position. The intersections between two circular regions have been measured by a circular division based on two neighboring vertebral cells, each of which is 65% of their area.

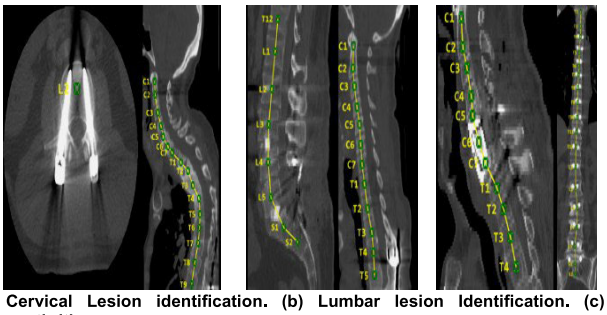

(a) Cervical Lesion identification. (b) Lumbar lesion Identification. (c) Osteoarthritis.

FIGURE 4. Weighted cervical and lumbar cases of the vertebral spine image.

This section discusses the steps in the path to our proposed spinal cord tumor assessment. In the first example, our approach uses vertical projection and normal vertebral distribution as follows.

- The cervical and lumbar lesion has been identified using vertical projection analysis.
- Second, we use boundary segmentation consisting of Gautschi's-Blur and HHTGM to establish the boundary between context and foreground.
- Third, vertebral position estimation is used to detect any vertebral poses in the image. Then we set up the T12 and L5 spine poses.

When T12 and L5 have been identified, T12-L1 and L4-L5 positions can be retrieved afterwards. Finally, to find bone injury, using the average intensity. All the parameter values used in the methods proposed are obtained from experiments.

Magnetic resonance imaging (MRI) showed in Figure 4, an extra modular intramural lesion in the film terminals region that fills the lumbar spinal canal and removes most of the signal strength of the normal cerebro-spinal fluid. Possibly due to encasement, the Conus modular and caudal equine did not clearly visualize. The whole lesion showed a significant improvement in contrast Figure 4 (a) and (b) in post-contrast T1 fat-saturated images as inferred from [22].

In the spinal axis Figure 4 (c) has shown no further improvement of focal soft tissue or osteoarthritis (OS). The lesion indicated an increase in the cystic concentration on the peripheral edges as indicated as in Figure 4 (b). Based on MRI imagery a differential diagnosis of an epidemic (most likely) or a tumor of the nerve sheath has been identified using HHTGM method.

B. MATHEMATICAL ANALYSIS-2: AN AVERAGE VERTICAL PROJECTION

The image of the vertebral spine is vertical. The cultivation of this work by vertical average intensity is an alternative way to identify the projection. Let R be an image input, $R(y, x_1)$ Which denotes pixel, y, x_1 gray levels. The average vertical projection is expressed as follows:

$$\gamma = \frac{1}{n} \sum_{y=1}^{pv} R(y, x_1) \tag{11}$$

Algorithm 2 Segmentation of Boundary Using Gautschi's-Blur (GB) Correction Model

1. ***Start Procedure: learning the segmentation of the boundary using Gautschi's-Blur correction model algorithm.***
   Begin
2. ***Input:*** y, x_1
3. ***Output*** γ
4. ***The vertebral average intensity of the original image is distributed as the form of normal distribution.***
5. ***Calculate*** $G(y \mid \gamma) = \frac{1}{\sqrt{2\mu}} e^{-\frac{(y-\gamma)^2}{2}}$.
6. ***Calculate*** $F(\theta) = \gamma T_u + F_{ext}(\theta)$
7. ***Calculate*** $F_{ext}(\theta) = \rho q_r(\theta) + \beta o_r(\theta)$
8. ***Calculate the energy coefficient functions of*** $q_r(\theta)$ ***and*** $o_r(\theta)$
9. ***Finally, determine average vertebral spine intensity VS***
10. ***End begin***
11. ***Until repeat for the entire strength in the backbone is equated of this average frequency and to find the bone damage.***
12. ***End procedure***

where, γ is the average intensity representation, pv denotes pixel vertical length, y *and* x_1 Represents horizontal and vertical length of the original image, respectively. The Vertebral average intensity of the original image is distributed in the form of normal distribution which is used to solve the data easily. Further the normal distribution function is defined as follows:

$$G(y \mid \gamma) = \frac{1}{\sqrt{2\mu}} e^{-\frac{(y-\gamma)^2}{2}} \tag{12}$$

As inferred from the Equation.12, γ is the average intensity representation that shows the mean (μ) variable G distribution. The contrast improvement method is used to facilitate the identification of the low resolution image. The post processing is a nonlinear process that encodes and decodes image luminance μ or tristimulus values, as defined as follows:

$$E_{out} = \mathrm{P}E_{in}^{\alpha} \tag{13}$$

where, P is the value of the constant which is equal to 1 and E_{in} Represents the inner ranging voltage from 0.1 to 0.6 and the value of $\alpha = 7$, if the alpha value is lesser than 1 which is termed as alpha encoding that makes the outer voltage brighter. Suppose if the alpha value is greater than 1 then it is called as alpha decoding that makes the outer voltage much darker than normal level.

C. MATHEMATICAL ANALYSIS-3: REGULARIZED DISTANCE SET (DS) OF EVOLUTION

As inferred From the Algorithm.2.

Step 1: Initially in the above algorithm learning the segmentation of boundary using Gautschi's-Blur correction model algorithm.

Step 2: Determine and execute the following parameters y, x_1 *and* γ

Step 3: Vertebral average intensity of the original image is distributed as the form of normal distribution and the average frequency is calculated using transforms which in turn reduce the number of required computations for processing the image in terms of series.

Step 4: Calculate G $(y \mid \gamma) = \frac{1}{\sqrt{2\mu}} e^{-\frac{(y-\gamma)^2}{2}}$.

Step 5: Determine F $(\theta) = \gamma T_u + F_{ext}(\theta)$

Step 6: Calculate $F_{ext}(\theta) = \rho q_r(\theta) + \beta o_r(\theta)$

Step 7: Calculate the energy coefficients functions of $q_r(\theta)$ and $o_r(\theta)$ and determine average vertebral spine intensity VS.

Step 8: Thus, the entire strength in the backbone is equated of this average frequency and to find the bone damage

As inferred from the algorithm. 2, the ultimate boundary of the spine is measured using this technique and this approach is described as the image frequency inhomogeneity. Here the related region from, inside and outside the contour to address this obstacle has been analysed using energy contour functional F (θ) which is represented as follows:

$$F(\theta) = \gamma b T_u + F_{ext}(\theta) \tag{14}$$

where, γb is the set of positive value and the first regulation level set is termed as T_u and it is defined as follows:

$$T_u = \int_{\delta}^{1} E_{out}(\Delta\theta)\mathrm{d}y \tag{15}$$

Therefore, the correlation of second external energy is termed as $F_{ext}(\theta)$ which depends on the correlation region between outside and inside of the contour as represented as δ, thus the external energy term is defined as follows:

$$F_{ext}(\theta) = \rho q_r(\theta) + \beta o_r(\theta) \tag{16}$$

When $\rho > 0$ and $\beta \ni \boldsymbol{\eta}$ are the energy coefficients functions of $q_r(\theta)$ and $o_r(\theta)$ which are defined as follows:

$$q_r(\theta) = \int_{\delta}^{1} E_{out}(\theta)(\Delta\theta)\mathrm{d}y \tag{17}$$

$$o_r(\theta) = \int_{\delta}^{1} E_{out}(\theta)(-\Delta\theta)\mathrm{d}y \tag{18}$$

A primary spinal vertebral tumor as shown in Figure 5 (a) and (b) are diagnosed in a spinal axis and in the absence of a lesion. If one or more histopathological confirmed primitive Neuro Vertebral tumor lesions are present, since most are secondary to primary current imaging is therefore analysed using the HHTGM diagnosis to rule out the possibility of metastasis from primary check. The clinical confirmation includes histopathological findings and a spinal injury, immune histochemical test is essential.

The black holes in most x-ray images vertebral bones are present. These black troughs are in the middle of the spine and the spinal position between the two black troughs with white spot identification as shown in the Figure 5 (c) and (d). This has been used to estimate the vertebral pose and thus the

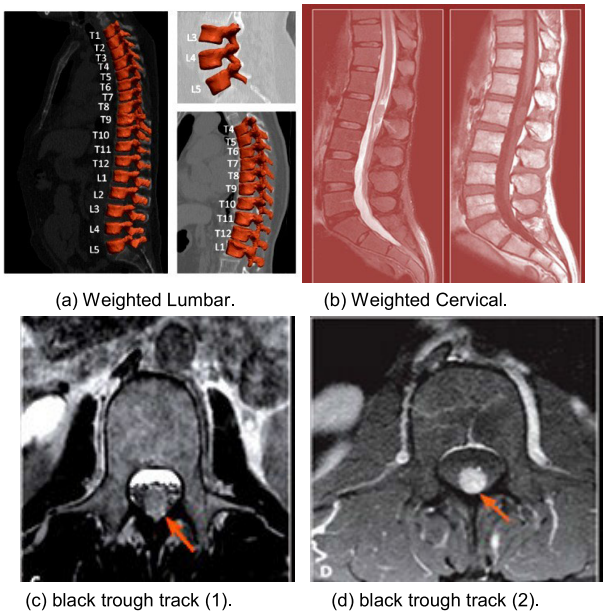

FIGURE 5. Difference of weighted cervical (WC) and lumbar cases of vertebral spine image.

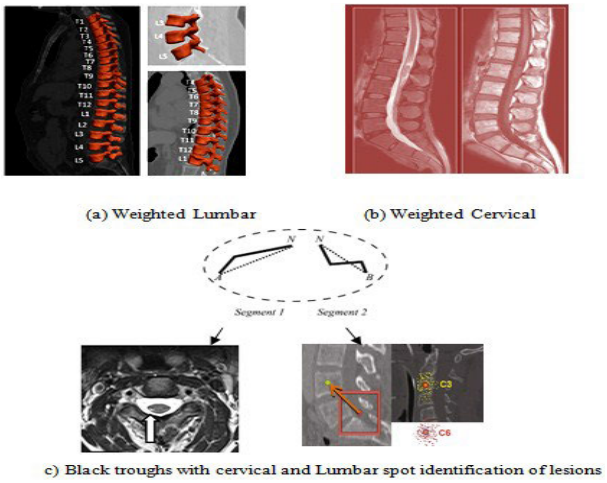

FIGURE 6. Difference of weighted cervical (C) and Lumbar cases of vertebral spine contrast image by using HHTGM algorithm with high precision.

Horizontal Summation (SH) of the position is determined as follows:

$$\mathrm{SH} = \sum_{x_2=1}^{m} k(y, x_2) \tag{19}$$

where, k is the black hole binary image, m represents the pixel horizontal length and (y, x_2) Denotes the horizontal and vertical length of an image.

Bone lesion is a symptom of a vertebral bone disease. It may, for example, contain calcium that is suggested by a high color or color intensity. The disease causes the bone mass density to be incorrectly measured by the radiologist. They calculate the average strength of the vertebral spine before the bone lesion region is found. The changed average vertebral spine intensity (VS) shall be defined as follows:

$$\mathrm{VS} = \frac{1}{b * m} \sum_{y=1}^{n} \sum_{x_2=1}^{m} S(y, x_2) \tag{20}$$

where, b is the width of vertical, and m is the width of horizontal. We may equate it with all the strength in the backbone of this average frequency and to find the black trough track which has been shown in the Figure 5 (c) and (d).

The second MRI follow-up study has found to be similar to the previous scan, and no significant changes have been made on the primary lesion site. Otherwise, the resulting marked compression of the cord has been reported to advance multiple intramural metastases in thoracic areas shown in Figure 6. The results show that the cord has been significantly compressed in a multi-level region of distance set as shown in the Figure 6 (a) and (b).

In comparison to the regressing metastatic lesion in the cervical area (thick, white arrow) as shown in the Figure 6 (c), several intra-dural metastases of the thoracic region (thin green and red spots with an arrow as shown in the Figure 6 (c) tended to grow has been identified with high precision (compared to Figure 5 which is shown in the above case). As these tumors develop inside the bone, they may likewise cause torment, vertebral breaks or spinal precariousness which has been further examined in this research using Internet of Medical things (IoMT) Platform. Whether harmful or not, a vertebral tumor can be hazardous and cause perpetual incapacity has been tentative and experimentally analysed in this research exploration. Imagine a world that communicates with billions of phones. There is a revolution waiting for these platforms, such as the sensors, actuators and intelligent Platform, in the healthcare industry as an internet of the things that can personalize health monitoring, diagnostic and treatment and reduce the cost of treatment. The most recent report on research the Internet of Medical Things in the Healthcare Market offers a pinpoint analysis of changing competitive dynamics and a perspective on the various factors driving or restricting the growth of the industry has been discussed below.

IV. RESULTS AND DISCUSSION

From 2013 to 2019, the health care market for Internet of Medical things is set to grow at a Compound annual growth rate (CAGR) of 56.27% [23]. This report analyses shown in Figure 7 the market and the future for investors or sellers who are prepared to exploit the market potential. The medial axis function or transform (MAT) operates on the medial axis or skeleton of the object. Mat can also be used for research purposes in health care. Thus, IoMT has a major effect in medical research which consists of Gate Way (GW) and IoT Cloud monitoring system. It allows larger and better treatments to be introduced. In a range of Platform, IoMT is used to improve the quality of the patient health care services.

The results have been computed based on the IoMT platform where the proposed numerical method HHTGM has been implemented. The study data have been based on the

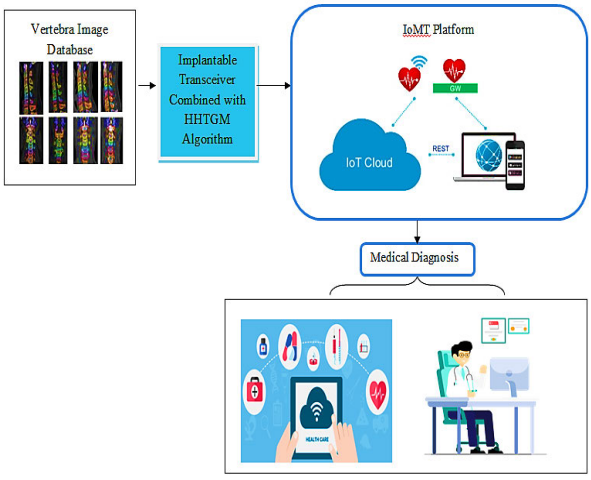

FIGURE 7. Fully automated image linked with IoMT platform.

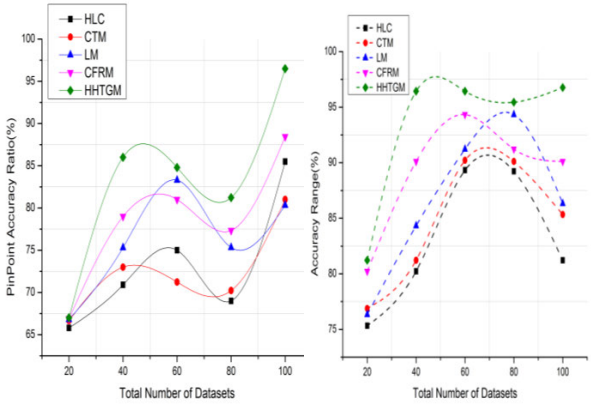

(a) PinPoint Accuracy Ratio for GB. (b) Accuracy Ratio for HHTGM.

FIGURE 8. Accuracy Analysis.

medically notable spine labels in two effective cervical and lumbar MRI pipelines [24]. Records have been obtained via the institution-wide electronic record search of 10 spine surgeons via surgical papers. The reports have been subsequently reviewed in clinical trials. Such results suggest that clinically collected image information can theoretically be used as training data for image analysis in pipelines such as HHTGM. Nevertheless, the annotations medications given need a quality assurance to ensure consistency because, as was initially found in this review, the annotation could not always be satisfactory or accurate.

The procedure provides a high dose of precisely directed radiation, which is not necessarily surgery. For Gautschi's-Blur (GB), doctors use machines to aim radiation beams from multiple angles on tumors with pinpoint accuracy ratio of GB shown in Figure 8 (a). In radio surgery, various types of equipment are used to administer radiation to treat vertebral tumors in a stereotactic manner. Here, the accuracy describes a mixture of both kinds (random and systematic) measurement errors. Furthermore, high accuracy demands for HHTGM as shown in Figure 8 (b). Since the border

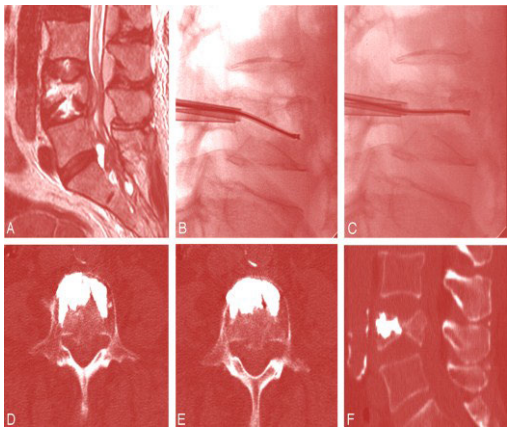

FIGURE 9. Detailed classification of labeling pipelines and trained detection result for cervical and lumbar MR images are analyzed based on the institution-wide electronic record search of 10 spine surgeons [22].

segmentation consisting of Gautschi's-Blur (GB) corrections and heuristic Hock transformations (HHTGM) to define the limits between the foreground and background increase the accuracy range in accordance with existing methods.

It consumed only a few seconds per case to achieve minimum effort. The complete annotation takes 5-15 Seconds per case load which can be compared with existing methods. While overall the time saved is modest in this scenario, the potential worth of complex annotations is evident. Note that the labeling pipeline has been applied, and very good results obtained for each case with an accuracy of 97.11 % for GB and 97.00% for HHTGM. Some of these detections might have been if several objects are processed as shown in Figure 9.

Successful findings shall be shown in Figure 9 (A) to (F). The labeling pipelines and trained detection result for cervical and lumbar MR images correspond to the annotated spine labeling on the qualified pipelines.

Such results show that existing image databases can be used further to provide added value as a source of in-depth learning information. The photographs in the archive and the associated notes are seldom accessed. Our results are consistent with those previously reported and exceed many of them, in particular in the case of location errors measured.

The location errors vary considerably from the findings of the noise analysis that is shown in Table 1 most recorded CT data sets with the biggest position errors for the whole spine and also for unspecified section of the spine is noted in the original image. Since P is the value of the constant which is equal to 1 and E_{in} Represents the inner ranging voltage from 0.1 to 0.6 and the value of $\alpha = 7$, if the alpha value is lesser than 1 which is termed as alpha encoding that makes the outer voltage brighter helps to reduce the noise value. Suppose if the alpha value is greater than 1 then it is called as alpha decoding that makes the outer voltage much darker than normal level with the noise range of 10.66 % to 5.3 %.

Based on the noise value, the imaging results are analysed with single radiographic sign and the nonspecific symptoms

TABLE 1. Noise analysis.

Number of Datasets	HLC	CTM	LM	CFRM	HHTGM
20	66.8	45.2	25.9	19.5	10.66
40	72.7	38.3	26.2	12.3	09.3
60	65.3	33.1	29.6	19.2	09.8
80	77.7	35.7	28.5	16.9	08.5
100	80.3	35.3	22.1	18.3	05.3

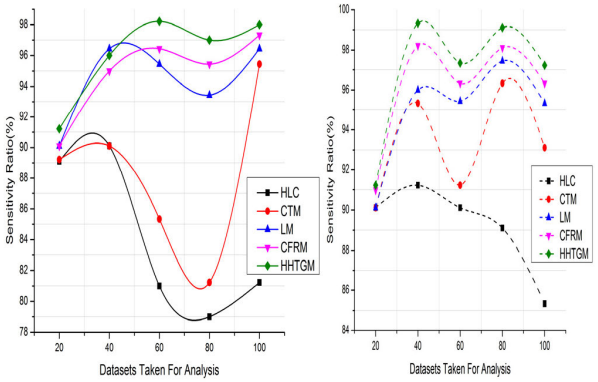

(a) Sensitivity Using GB Model Using HHTGM. (b) Sensitivity

FIGURE 10. Sensitivity validation.

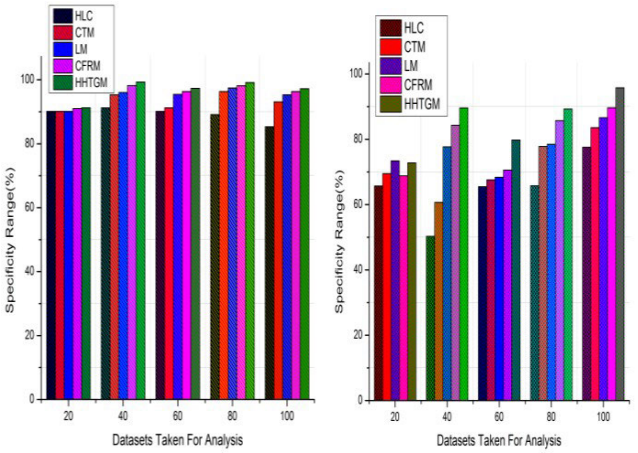

(a) Specificity Using GB Model Using HHTGM. (b) Specificity.

FIGURE 11. Specificity analysis.

TABLE 2. Mean square error.

Number of Datasets	HLC	CTM	LM	CFRM	HHTGM
20	7.35	7.04	6.99	6.75	6.26
40	7.02	7.53	5.42	5.23	5.19
60	6.62	6.02	6.96	5.92	5.12
80	7.27	6.87	6.45	5.59	4.55
100	6.47	5.99	5.98	5.83	4.51

of radiography exist shown in Figure 10 (a). By contrast to traditional angiography, HHT can be more dissection sensitive than MRI or ultrasound. Since the principle of the Heuristic Hock Transform (HHT) is used as a reference point in the HT space which is defined based on the position of the target contour. The HHT transformation, kernel has been defined as the HT derivative helps to improve the sensitivity ratio 98.2% for GB and 99.3% for HHTGM as shown in the Figure 10 (a) and (b).

As inferred from the Figure 10 (b), Since the scale factor, fix clockwise, and the translations described by y and x respectively which are represented by $b_y(s)$ and $b_x(s)$. The principle of the Heuristic Hock Transform (HHT) is used as a reference point in the HT space which is defined based on the position of the target contour helps to improve the sensitivity.

Figure 11 (a) shows the radiological characteristics in the manuscripts included and their relative frequencies with specificity. The reported frequencies of these findings were quite inhomogeneous, as demonstrated by the large standard errors. 51% of individuals with HHGTM registered vertebral spines and there was at least one radiography "leading" finding in 15%. Since the regions of the center of the vertebral cell have been measured by the circulation size of smaller areas around each spine marking position. The intersections between two circular regions have been measured by a circular division based on two neighboring vertebral cells, each of which is 98.33% of their area with high specificity for GB and HHTGM as shown in the Figure 11 (a) and (b). Since image findings for individuals without vertebral spine have been reported in these reviewed studies to calculate the specificity of these image findings for HHTGM diagnosis as represented in Figure 11 (b).

This is no surprise as it is much harder to detect and mark arbitrary parts of the spine than to perform a particular full spine segment, such as the cervical or lumbar spine. It is worth noting that our results are reported on the basis of 2D distances for the localization fault while certain results in Table 2 are based on the 3D distances that may be slightly larger.

As inferred from the Table 2, HHTGM has minimum mean square error which about 4.51%. The boundary of the spine is

TABLE 3. Overall efficiency of HHTGM method.

Number of Datasets	HLC	CTM	LM	CFRM	HHTGM
20	65.7	69.5	73.4	68.8	72.8
40	50.3	60.7	77.7	84.3	89.6
60	65.5	67.6	68.4	70.6	79.8
80	65.8	77.8	78.5	85.7	89.3
100	77.6	83.6	86.6	89.7	95.8

measured using this technique and this approach is described as the image frequency inhomogeneity. Here, the related region from, inside and outside the contour to address this obstacle has been analysed using energy contour functional F (θ) reduce the mean square error. There can be an interesting comparison between the annotations and crowd sourcing provided clinically. Multi-sourcing is often referred to as a process where a crowd, usually online, voluntarily carries out or provides financial support for a project. This was used as an example for supplying large quantities of profound learning training data. Crowd sourcing has succeeded in providing better efficiency in medical imaging of the vertebral spine using IoMT shown in Table 3.

As inferred From the Table 3, the medical supplied annotations can be used as a form of training data given by individuals, while radiologists provide them as normal work. Since, the centroids of the detections have been maintained and supplied with a partially derived graphic template that follows the connecting components analysis of the detection charts, which rejects false positive detection and marks remaining detection with high efficiency about 95.8%.

Since, the vertical average intensity is an alternative way to identify the projection. Let R be an image input, $R(y, x_1)$ Which denotes pixel, y, x_1 Grey levels with high precision.

As inferred from the Figure 12, HHTGM has maximum precision which about 99.4%. The findings of the failed detections were either associated with missing detections triggered by pathologies or partly occult vertebrates. For example, when S1 detection was missing or when S2 had been confused, and some vertebras were not seen in an image in the mid-sagittal. As the Heuristic Hock Transform (HHT) is used as a reference point in the HT space which is defined based on the position of the target contour with high precision value.

The failure detection is shown in Figure 13. For cervical cases, the error rate of 4.5% localization error rate has been reported to the lumbar case length. This is clarified largely by the substantially lower cervical than the lumbar vertebrae, which decreases the difference in position. The accuracy of the labeling of 97 % to 98% is expected since improper labeling is the direct result of failed detections.

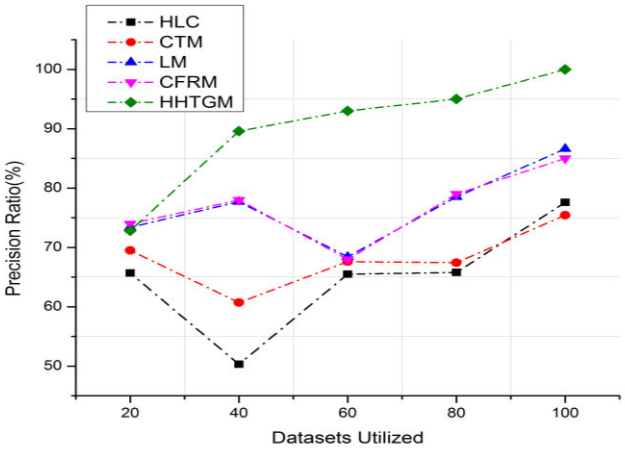

FIGURE 12. Precision ratio by HHTGM algorithm.

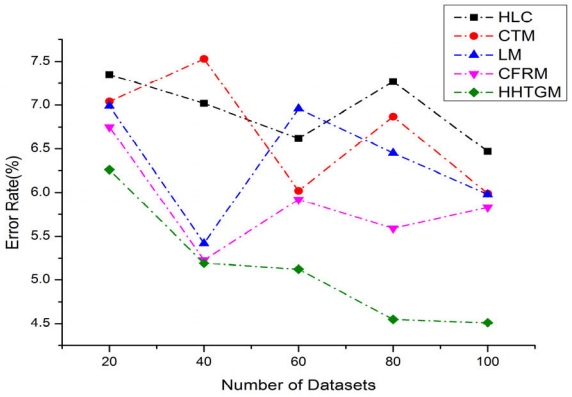

FIGURE 13. Error rate using HHTGM algorithm.

In future, Additional CNNs, training to identify the transitions C7/T1 and T12/L1, are also required to control these conditions, and multiple 2D images, or even 3D image volumes like ribs, are most likely to have to be considered. The findings reported often limit the amount of information used for the progress assessment of automatic vertebral detection and labeling. The robustness, reliability and transferability of new data to patients and other entities must be further verified.

V. CONCLUSION

A new approach of two issues with bone damage in the low-resolution backbone of radiation images has been suggested in this paper. The first problem involves the removal of separate vertebral objects: T12 and L5. Secondly, bone damages the vertebral spine is identified. Our approach proposed is able to try to classify objects of interest to a fair low resolution image. Our suggested solution is based on vertical projection and normal distribution automatically cropping the spine. Afterwards, Gautschi's-Blur Correction and the HHTGM system detect the vertebral spine line. To find a vertebral posture and remove T12, the segmentation method will be used vertebral pose estimate using IoMT systems. Ultimately, the solution proposed could automatically detect bone lesions

with the increase in average frequency. An expert radiologist compared the results of our approach to the basic truth. The experimental analysis in accordance with HLC, CTM, LM, and CFRM, moreover HHTGM in this research explored the best results with 95.8% efficiency and 98.66 % of precision when compared with other methods.

REFERENCES

[1] M. Neo, S. Fujibayashi, M. Miyata, M. Takemoto, and T. Nakamura, "Vertebral artery injury during cervical spine surgery: A survey of more than 5600 operations," *Spine*, vol. 33, no. 7, pp. 779–785, 2008.

[2] W. T. Edwards, Y. Zheng, L. A. Ferrara, and H. A. Yuan, "Structural features and thickness of the vertebral cortex in the thoracolumbar spine," *Spine*, vol. 26, no. 2, pp. 218–225, 2001.

[3] J. W. M. Kouwenhoven, K. L. Vincken, L. W. Bartels, R. M. Castelein, "Analysis of preexistent vertebral rotation in the normal spine," *Spine*, vol. 31, no. 13, pp. 1467–1472, 2006.

[4] Z. Y. C. Liu, J. H. Moxley, P. Kanive, A. C. Gleiss, T. Maughan, L. Bird, O. J. D. Jewell, "Deep learning accurately predicts white shark locomotor activity from depth data," A*nimal Biotelemetry*, vol. 7, no. 1, pp. 1–13, 2019.

[5] C. Bauer, D. M. Black, P. Garnero, M. Hochberg, S. Ott, J. Orloff, D. E. Thompson, S. K. Ewing, P. D. Delmas, and Fracture Intervention Trial Study Group, "Change in bone turnover and hip, non-spine, and vertebral fracture in alendronate-treated women: The fracture intervention trial," *J. Bone Mineral Res.*, vol. 19, no. 8, pp. 1250–1258, 2004.

[6] D. Mitra, V. N. Cassar-Pullicino, and I. W. Mccall, "Longitudinal study of vertebral type-1 end-plate changes on MR of the Lumbar Spine," *Eur. Radiol.*, vol. 14, no. 9, pp. 1574–1581, 2004.

[7] T. H. Dewangga, V. H. P. Suryanta, and H. Herman, "Hubungan antara akseptabilitas X-ray servikal lateral dengan tingkat kesadaran dari pasien cedera kepala di RS Hasan sadikin," *Tunas Medika Jurnal Kedokteran Kesehatan*, vol. 5, no. 3, pp. 11–14, Oct. 2019.

[8] G. Li, S. Wang, P. Passias, Q. Xia, G. Li, and K. Wood, "Segmental in vivo vertebral motion during functional human lumbar spine activities," *Eur. Spine J.*, vol. 18, no. 7, pp. 1013–1021, 2009.

[9] J. Chmelik, R. Jakubicek, J. Jan, P. Ourednicek, L. Lambert, E. Amadori, and G. Gavelli, "Fully automatic CAD system for segmentation and classification of spinal metastatic lesions in CT data," in *Proc. World Congr. Med. Phys. Biomed. Eng.* Singapore: Springer, 2018, pp. 155–158.

[10] C. Wong, J. Hall, and K. Gosvig, "The effects of rotation on radiological parameters in the spine," *Acta Radiol.*, vol. 60, no. 3, pp. 338–346, 2019.

[11] C. W. Peng, B. T. Chou, J. A. Bendo, and J. M. Spivak, "Vertebral artery injury in cervical spine surgery: Anatomical considerations, management, and preventive measures," *Spine J.*, vol. 9, no. 1, pp. 70–76, 2009.

[12] C. Parenteau, S. Holcombe, P. Zhang, C. Kohoyda-Inglis, and S. Wang, "The effect of age on fat and bone properties along the vertebral spine," *SAE Int. J. Transp. Saf.*, vol. 1, no. 2, pp. 226–240, 2013.

[13] O. Tsiakaka and S. Feruglio, "Toward the monitoring of the spinal cord: A feasibility study," *Microelectron. J.*, vol. 88, pp. 145–153, Jun. 2019.

[14] K. Morita, T. Nakaura, N. Maruyama, Y. Iyama, S. Oda, D. Utsunomiya, T. Namimoto, M. Kitajima, M. Yoneyama, and Y. Yamashita, "Hybrid of compressed sensing and parallel imaging applied to three-dimensional isotropic T2-weighted turbo spin-echo MR imaging of the Lumbar Spine," *Magn. Reson. Med. Sci.*, to be published.

[15] S. Ebrahimi, L. Gajny, W. Skalli, and E. Angelini, "Vertebral corners detection on sagittal X-rays based on shape modelling, random forest classifiers and dedicated visual features," *Comput. Methods Biomech. Biomed. Eng., Imag. Vis.*, vol. 7, no. 2, pp. 132–144, 2019.

[16] I. M. G. Jakobsen and M. Plocharski, "Automatic detection of cervical vertebral landmarks for fluoroscopic joint motion analysis," in *Proc. Scand. Conf. Image Anal.* Cham, Switzerland: Springer, Jun. 2019, pp. 209–220.

[17] K. Yokota, T. Maeda, O. Kawano, E. Mori, T. Takao, H. Sakai, and M. Masuda, "Progression of local kyphosis after conservative treatment for compressive cervical spine fracture with spinal cord injury," *J. Orthopaedic Surg. Res.*, vol. 14, no. 1, p. 98, 2019.

[18] S. R. Cummings, D. B. Karpf, F. Harris, H. K. Genant, K. Ensrud, A. Z. LaCroix, and D. M. Black, "Improvement in spine bone density and reduction in risk of vertebral fractures during treatment with antiresorptive drugs," *Amer. J. Med.*, vol. 112, no. 4, pp. 281–289, 2002.

[19] H. Milavec, C. Kellner, N. Ravikumar, C. E. Albers, T. Lerch, S. Hoppe, M. C. Deml, S. F. Bigdon, N. Kumar, and L. M. Benneker, "First clinical experience with a carbon fibre reinforced PEEK composite plating system for anterior cervical discectomy and fusion," *J. Funct. Biomater.*, vol. 10, no. 3, p. 29, 2019.

[20] S. Appel, T. Biron, K. Goldstein, and E. Ashkenazi, "Effect of intra-and extraoperative factors on the efficacy of intraoperative neuromonitoring during cervical Spine surgery," *World Neurosurg.*, vol. 123, pp. e646–e651, Mar. 2019.

[21] Accessed: Oct. 10, 2019. [Online]. Available: http://spineweb.digitalimaginggroup.ca/spineweb/index.php?n=Main.Datasets

[22] Accessed: Oct. 10, 2019. [Online]. Available: https://biomedia.doc.ic.ac.uk/data/spine/

[23] Accessed: Oct. 10, 2019. [Online]. Available: https://www.orbisresearch.com/reports/index/internet-of-things-in-healthcare-applications-devices-analytics-smart-products-growth-trends-and-forecasts-2017-2022

[24] M. Seif, C. A. M. G. Wheeler-Kingshott, J. Cohen-Adad, A. E. Flanders, and P. Freund, "Guidelines for the conduct of clinical trials in spinal cord injury: Neuroimaging biomarkers," *Spinal Cord*, vol. 57, no. 9, pp. 717–728, 2019.

HASSAN FOUAD studied mechanical engineering at Helwan University, Egypt. He received the B.Sc. and M.Sc. degrees in 1990 and 1996, respectively, and the Ph.D. degree in biomedical polymers from the University of Leeds, U.K., and Helwan University, in 2000. He was as a Research Scientist with the Vienna University of Technology. He is currently a Full Professor of biomaterials and tissue engineering with King Saud University and Helwan University.

AZZA S. HASSANEIN received the bachelor's degree in biomedical engineering from Helwan University, Cairo, Egypt, in 2004, the master's degree in biomedical engineering from Cairo University, Cairo, in 2009, and the Ph.D. degree in biomedical engineering from Helwan University, in 2015. She is currently an Assistant Professor in biomedical engineering with Helwan University. She is also a Researcher with JMI at New Delhi, India.

AHMED M. SOLIMAN received the B.Sc. (Hons.), M.S., and Ph.D. degrees in biomedical engineering from Helwan University, Cairo, Egypt, in 2003, 2010, and 2017, respectively, and the M.S. degree in biotechnology engineering from the University of Chemical Technology and Metallurgy (UCTM), Sofia, Bulgaria, in 2009. From 2010 to 2012, he was an Exchange Ph.D. Student with the Biophotonics Group, Lund Medical Laser Centre, Atomic Physics Division, Physics Department, Faculty of Engineering (LTH), Lund University, Lund, Sweden. He is currently an Assistant Professor with the Biomedical Engineering Department, Faculty of Engineering, Helwan University.

HAYTHAM AL-FEEL received the B.Sc. degree from the Faculty of Engineering, Quarter University, and the Ph.D. degree from the College of Electronic Engineering, Menofia University, Egypt. He is currently an Associate Professor with the Faculty of Computers & Information, Fayoum University.